Chinese Chemical Letters 37 (2026) 111264

Contents lists available at ScienceDirect

Chinese Chemical Letters

journal homepage: www.elsevier.com/locate/cclet

Pressure-enhanced self-trapped exciton emission in stereochemically active $SbTaO_4$

Dequan Jiang[a], Long Zhang[a], Chen Li[b], Ke Liu[b], Yingying Ma[b], Hao-Ming Cheng[b], Tianyao Pei[b], En Chen[b], Jianbo Zhang[b], Ting Wen[b], Yang Ding[b], Yonggang Wang[a,*]

[a] State Key Laboratory of Advanced Waterproof Materials, School of Materials Science and Engineering, Peking University, Beijing 100871, China
[b] Center for High Pressure Science and Technology Advanced Research (HPSTAR), Beijing 100193, China

ARTICLE INFO

Article history:
Received 23 February 2025
Revised 20 April 2025
Accepted 27 April 2025
Available online 27 April 2025

Keywords:
STE emission enhancement
Non-radiative transitions
Electron-phonon coupling
Hindered transition
Structural distortion

ABSTRACT

Self-trapped exciton (STE) emissions based on Sb^{3+} ion materials have recently received widespread attention, due to the excellent photoluminescence (PL) properties and stereochemical activity of Sb^{3+} ions. Pressure can precisely regulate the electronic structure and configuration of chromophores, becoming an effective approach to enhance the STE emissions. Recently, STE emission enhancements in Sb^{3+}-based materials under pressure mainly focus on metal halides, however, studies on inorganic oxides are very limited. Herein, the high-pressure STE behavior of $SbTaO_4$ was investigated up to 13.2 GPa. The STE emission exhibits a bi-peak feature, and the strongest emission occurs at 3.8 GPa, in which two peaks are enhanced by ~20 and ~3 times and the STE emission displays a bright green color. The mechanism is explained using a variety of methods, including steady-state PL spectroscopy, kinetic spectroscopy, Raman spectroscopy, cryogenic PL spectroscopy and theoretical calculations. It shows that the strong electron-phonon coupling of $SbTaO_4$ is weakened, which suppresses non-radiative transitions. Also, the distortion of the $[SbO_4]$ unit inhibits the transition between two STE states. The synergistic effect of these factors leads to a strong enhancement of the STE emission in $SbTaO_4$ under pressure. The STE emission enhancement of $SbTaO_4$ highlights the potential of inorganic oxides for future high-pressure STE exploration and provides the promising material in photonic devices under extreme conditions.

© 2026 Published by Elsevier B.V. on behalf of Chinese Chemical Society and Institute of Materia Medica, Chinese Academy of Medical Sciences.

Self-trapped exciton (STE) emission has garnered significant attention due to its unique photoluminescence (PL) properties and potential applications in phosphors, light-emitting diodes, and scintillators [1–4]. STE emissions typically arise in systems with strong electron-phonon coupling, where lattice distortions caused by excited electrons and holes rapidly trap them in lower-energy self-trapped states, as opposed to free carrier states [5–8]. Recently, the STE emission phenomenon is widely observed in ns^2 metal ion-based material systems, in which the lone-pairs electrons (LPEs) of ns^2 metal ion are generally stereochemically active [9,10]. Among the various ns^2 metal ion-based materials, those containing Sb^{3+} ions are particularly promising [11–13]. The $5s^2$ LPEs of Sb^{3+} ions not only offer broad-band emission and large Stokes shifts, which can avoid self-absorption effectively, but also exhibit remarkable chemical reactivity, attributed to their stereochemical activity and structural flexibility [14–16]. Furthermore, Sb^{3+} ions are recognized for their tunable blue, green, and red luminescence, positioning them as low-toxicity, highly stable candidates for a wide range of optical applications [17–19]. Currently, research on Sb^{3+}-based STE emission materials is primarily focused on metal halides systems, attributed to factors such as their flexible lattice structure and strong electron-phonon coupling [11,14,20–23]. However, compared to metal halides, inorganic oxides possess higher physical and chemical stability, yet the exploration of Sb^{3+}-based inorganic oxides remains relatively limited.

Precise structural modulation offers an effective approach to optimizing the STE emissions of materials [11,24,25]. Compared to introducing chemical pressure *via* doping within the crystal structure, applying external pressure provides a more direct method to influence the chromophores [26–29]. Previous reports have investigated significant STE emission enhancements through pressure-tuning the coordination environment of the chromophores in low-efficiency PL materials [30–35]. The presence of LPEs in Sb^{3+} ions causes an unsaturated coordination environment, imparting significant flexibility to the forming coordination polyhedra. Recently, pressure-induced distortion of Sb^{3+}-based polyhedra in low-dimension hybrid metal halides have been an

* Corresponding author.
E-mail address: ygw@pku.edu.cn (Y. Wang).

https://doi.org/10.1016/j.cclet.2025.111264
1001-8417/© 2026 Published by Elsevier B.V. on behalf of Chinese Chemical Society and Institute of Materia Medica, Chinese Academy of Medical Sciences.

effective strategy to obtain high-intensity and variable-energy STE emissions [16,36,37]. Relatively, in Sb^{3+}-based inorganic oxide system, many materials exhibit significant electron-phonon coupling [38–40]. Pressure can be used as a means to modulate the electron-phonon coupling and the coordination environment, further influencing their STE emissions. Based on the scarcity of research on Sb^{3+}-based inorganic oxides, it is worth exploring the evolution of the STE emissions under pressure.

$SbTaO_4$ is a polar material [41,42], in which Sb^{3+} ions exhibit stereochemical activity, and is potentially capable of the STE behavior. Combined with high-pressure technology, the phenomenon of pressure-driven STE emission enhancement in $SbTaO_4$ was reported. Under ambient condition, $SbTaO_4$ exhibits weak singlet STE emission, and this STE emission is enhanced up to ~20 times under pressure, which shows the strong green emission. Multiple *in situ* high-pressure techniques, including steady-state PL spectroscopy, kinetic transient absorption spectroscopy, local structure analysis, have been employed to reveal the mechanism of the emission enhancement, which is caused by the suppression of non-radiative transitions and the hindered transition between two STE states. The discovery of the strong STE emission enhancement in $SbTaO_4$ shed light on the future high-pressure exploration of the STE emissions in inorganic oxides, and provide potential materials for precision photonic devices under high pressure.

$SbTaO_4$ crystallizes in the polar space group $Pbn2_1$, featuring two types of distorted polyhedra: the LPE [SbO_4] unit and the second-order Jahn-Teller [TaO_6] polyhedron (Fig. 1a). The LPE [SbO_4] units connect through edge-sharing to form one-dimensional chains, while the [TaO_6] polyhedra connect through vertex-sharing to create a two-dimensional layer. These two structures alternate, forming the three-dimensional crystal structure of $SbTaO_4$. Powder sample of $SbTaO_4$ was obtained through high-temperature solid-state reaction under vacuum condition, with its purity confirmed by X-ray diffraction analysis (Fig. S1a in Supporting information). Scanning electron microscopy (SEM) revealed that the particle size of the powder sample was approximately 500 nm (Fig. S1b in Supporting information). Energy dispersive X-ray spectroscopy indicated that the atomic ratio of Sb, Ta, and O was 1.05:1:4.4, aligning well with the expected stoichiometry (Fig. S2 in Supporting information). In addition, X-ray photoelectron spectroscopy was performed to verify the oxidation states of Sb and Ta atoms (Fig. S3 in Supporting information). Characteristic peaks at 530.60 and 26.50 eV were attributed to Sb^{3+} $3d_{5/2}$ and Ta^{5+} $4f_{7/2}$, respectively, consistent with the proposed structural model. Recently, LPE Sb^{3+} ions have been generally introduced into crystal structures to achieve materials with excellent PL properties due to their ability to produce the STE emission. Polar materials often exhibit strong electron-phonon coupling effects, which result in significant non-radiative transitions and establish weak PL efficiency. Therefore, the polar material $SbTaO_4$ is anticipated to exhibit novel PL phenomena through pressure modulation.

$SbTaO_4$ has been reported to exhibit broad PL emission at low temperatures, which also indicates that $SbTaO_4$ shows no PL emission at room temperature [43]. In this paper, the high-intensity lasers were used as the excitation lights to observe the PL emission behavior at room temperature and conducted investigations under pressure. Using lasers with wavelengths of 375 and 405 nm to excite powder $SbTaO_4$, respectively, it was found that both broad PL emissions exhibited in the range of 400–800 nm (Fig. 1b and Fig. S4 in Supporting information). The position and shape of two PL emissions basically remain unchanged regardless of the variation in the excitation light energy, which is a characteristic of the STE emission mechanism [16]. Meanwhile, it was observed that the PL emission exhibited bi-peak characteristics. By employing Gaussian fitting, the PL emission excited by 405 nm laser was processed into two independent peaks I and II. The positions of two

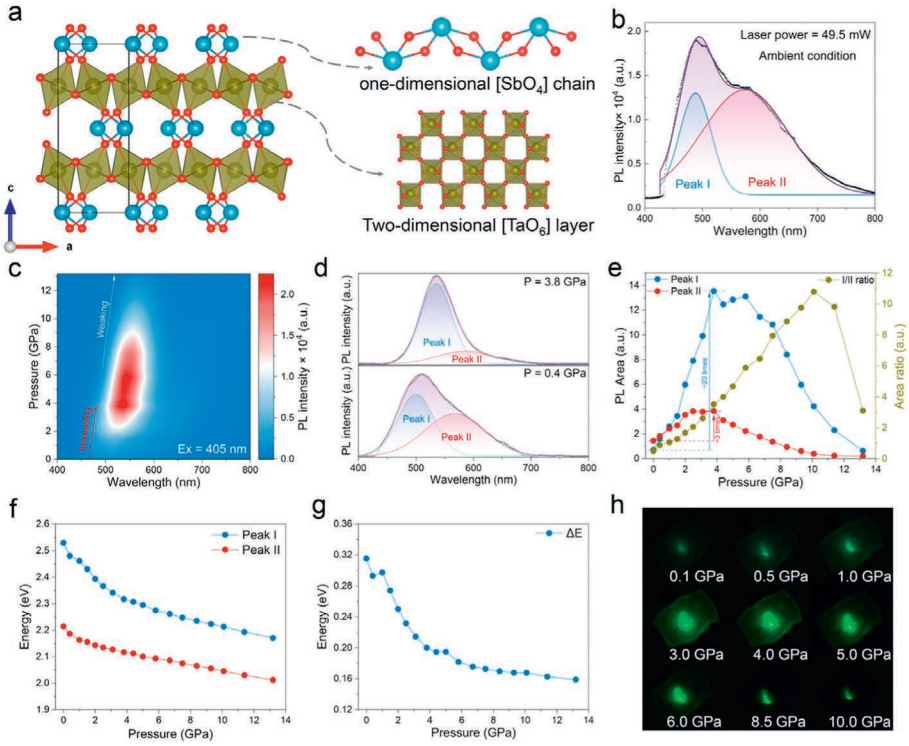


Fig. 1. (a) Crystal structure of $SbTaO_4$. (b) The PL spectrum using the excitation at 405 nm with the laser power of 49.5 mW under ambient condition. (c) Pressure-dependent *pseudo*-color PL spectra using the excitation at 405 nm under room temperature. (d) The PL spectra under 0.4 GPa and 3.8 GPa. (e) The area evolutions of peak I and peak II under pressure. (f) Energy evolutions of the peak I and peak II emissions. (g) The energy difference (ΔE) between the peak I and peak II emissions. (h) Selected high-pressure optical micrographs using the excitation at 405 nm.

peaks are 488 and 574 nm, respectively, and all process broad full-widths at half-maximum (FWHM) of 0.34 and 0.67 eV, according to the different emission energy, peak I and peak II emissions can be attributed to the transitions of high-energy self-trapped exciton (HP STE) and low-energy self-trapped exciton (LP STE), respectively. Such large Stokes shifts and broad FWHMs confirm that the PL emission of $SbTaO_4$ belongs to the STE emission mechanism. In addition, power-dependent PL measurements were also performed (Fig. S5 in Supporting information), which showed that the peak intensity of peak I and peak II exhibits a linear relationship with the laser power, excluding the mechanism of permanent defect emissions [16,44,45].

High-pressure PL property studies on $SbTaO_4$ revealed a significant PL enhancement phenomenon using 405 nm laser as excitation light source (Fig. 1c and Fig. S6 in Supporting information). Totally, the PL emission process can be divided into three stages: (1) The PL emission rapidly increased within the range of 0−3.8 GPa; (2) The PL emission remained stable within the range of 3.8−5.8 GPa; (3) The PL emission continuously weakened within the range of 5.8−13.2 GPa. As the bi-peak characteristic of the STE emission, the evolutions of peak I and peak II were also investigated in detail by Gaussian fitting. As shown in Fig. 1d, under low pressure, peak II is dominant in the whole PL emission. With pressure increasing, peak I emission increases faster, gradually surpassing peak II and becoming dominant. The evolution trend is quantified by the statistic of the PL peak areas and area ratio (Fig. 1e). It can be observed that the areas of peak I and peak II both undergo a process of first increasing and then decreasing. The maximum enhancement occurs at 3.8 GPa which is ~20 times and ~3 times for peak I and peak II, respectively. The area ratio of peak I to peak II increases from 0.5 at ambient pressure to 10.8 at 10.1 GPa, which indicates that the emission process of peak I is more promoted compared to peak II. In addition, the energy evolution of peak I and peak II was also analyzed, and it was observed that the energy difference (ΔE) between peak I and peak II was continuously decreasing (Figs. 1f and g). This phenomenon implied the lifted degeneracy of two emission states, which should be attributed to the increased trapping barrier between two emission states [16]. The increased trapping barrier hindered the transition of excitons from HP STE to LP STE, leading to more excitons transitioning from HP STE to the ground state, which is the potential reason for the significant enhancement of peak I under pressure. The hindrance of exciton transition will be further discussed later. The PL micrographs (Fig. 1h), intuitively displays the PL emission evolution. It clearly displays that $SbTaO_4$ exhibits the green emission and experiences the process of the PL emission from enhancement, stability to weakening. The PL spectrum after pressure release was also collected, revealing that the PL intensity of $SbTaO_4$ after pressure release is slightly weaker than that before pressurization (Fig. S7 in Supporting information). This can be attributed to the reduction of the crystallinity caused by pressure during the compression process.

To further understand the PL emission mechanism of $SbTaO_4$, high-pressure time-resolved PL decay measurements were performed (Figs. 2a–c). The high-pressure decay curves can be fitted well by three-index exponential function, $I_{(t)} = I_{(0)} \cdot [A_1 \cdot \exp(-t/\tau_1) + A_2 \cdot \exp(-t/\tau_2) + A_3 \cdot \exp(-t/\tau_3)]$, and the average lifetimes τ_{AvInt} were also obtained according to the function $\tau_{AvInt} = [A_1\tau_1^2 + A_2\tau_2^2 + A_3\tau_3^2]/[A_1\tau_1 + A_2\tau_2 + A_3\tau_3]$. The nanosecond-scale time of the PL emission indicates that the transition mode is a singlet-to-ground state transition process, which is the $^1P_1 - {}^1S_0$ transition due to spin-orbit coupling in Sb^{3+} ions [11]. The singlet lifetime of $SbTaO_4$ is shorter than the most reports of singlet Sb^{3+} states, which usually have the lifetimes on the order of 10 ns, while it can be compared with the Sb^{3+}-coordination complex, $[Sb_2O(PDC)_2(H_2O)_2]$, in which its lifetime of singlet emission is considered to be 3.2 ns [46]. Under pressure, the average lifetimes τ_{AvInt} initially increases rapidly, and then the rate of increase slows down around 4.2 GPa, finally stabilizing at about 1.5 ns. The increase in τ_{AvInt} is due to the fact that all three lifetimes (τ_1, τ_2, τ_3) exhibit an increasing trend under pressure. Totally, the evolution of the PL decay times can

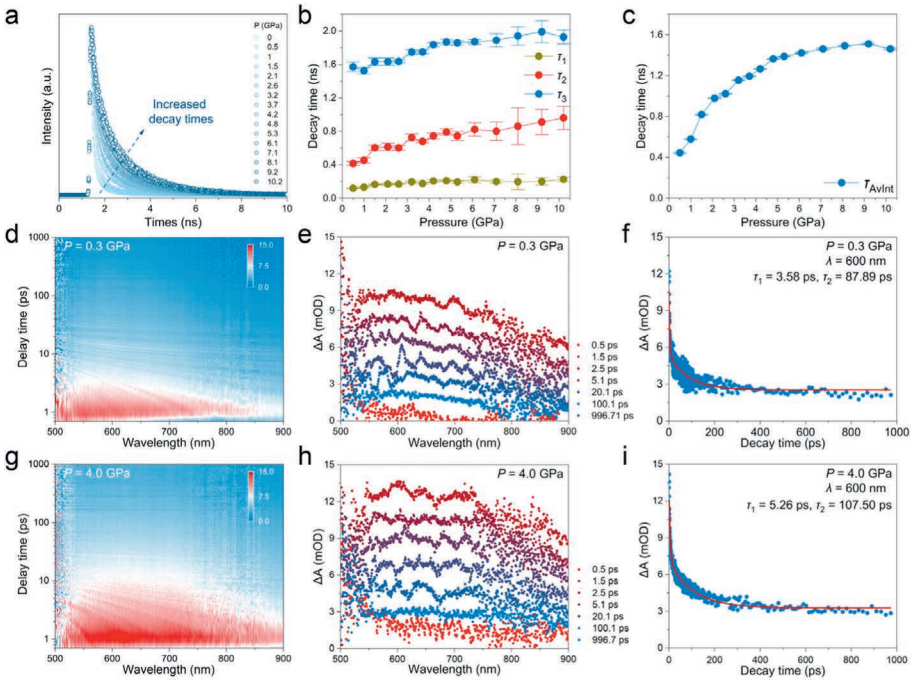


Fig. 2. (a) PL decay time curves under pressure. (b) Decay time evolutions of τ_1, τ_2, τ_3. (c) Pressure dependence of the average dacay times τ_{AvInt}. (d) *Pseudo*-color TA plot under 0.3 GPa. (e) The selected TA spectra. (f) Decay dynamics probed at 600 nm. (g) *Pseudo*-color TA plot under 4.0 GPa. (h) The selected TA spectra. (i) Decay dynamics probed at 600 nm.

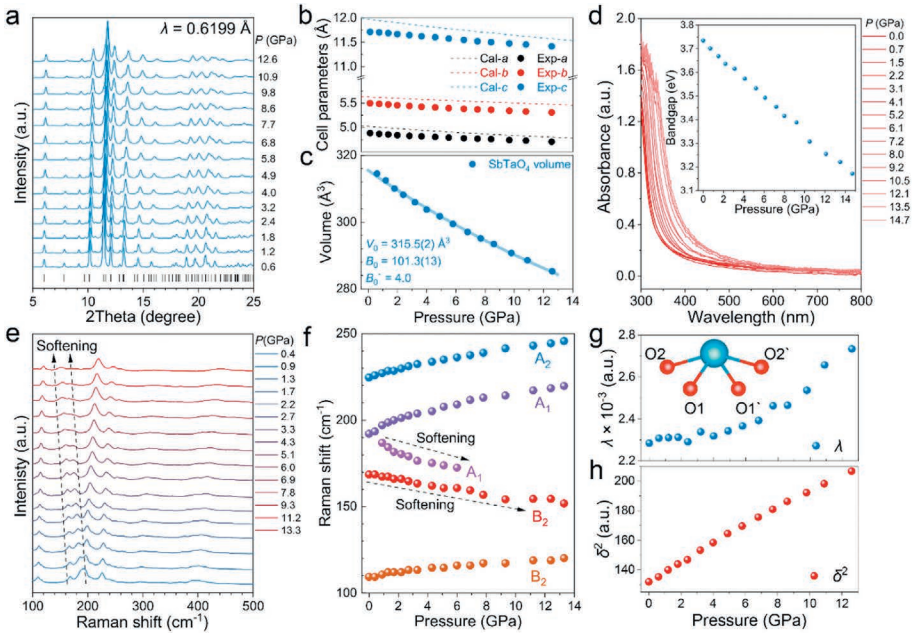


Fig. 3. (a) High-pressure XRD patterns. (b) Calculated and experimental cell parameters as a function of applied pressure. (c) Pressure dependence of cell volumes and the second-order Birch-Murnaghan equation of state fitting. (d) High-pressure evolutions of absorption spectra and bandgaps. (e) High-pressure Raman patterns. (f) Pressure dependence of the Raman peak positions. High-pressure evolution of (g) bond-length deviation of λ and (h) bond-angle deviation of δ^2 using geometry optimization.

be caused by the factors [47,48], such as non-radiative transitions, excited-state structural evolutions, which will be further discussed by the following measurements.

High-pressure femtosecond transient absorption (TA) spectroscopy of $SbTaO_4$ was also employed to further analyze the evolution of STE emission under pressure (Figs. 2d–i). With 405 nm laser excitation, a broad positive photo-induced absorption was observed among the wavelength of 500–900 nm for $SbTaO_4$ under 0.3 and 4.0 GPa, respectively, which is the characteristic of the STE emission [49,50]. Comparing the TA spectra, it can be clearly observed that the positive photo-induced absorption enhanced under pressure and the decay times at 4.0 GPa became longer than that at 0.3 GPa. Furthermore, the decay times at 600 nm were fitted using the two-index exponential function. The lifetimes at 4.0 GPa ($\tau_1 = 5.26$ ps, $\tau_2 = 107.50$ ps) are consistently longer than lifetimes ($\tau_1 = 3.58$ ps, $\tau_2 = 87.89$ ps) at 0.3 GPa. The longer lifetimes of $SbTaO_4$ under pressure imply the increased radiative recombination and suppressed non-radiative process in $SbTaO_4$, referred to inorganic halide double perovskites that achieve the STE emission enhancement by cation doping [51].

High-pressure synchrotron powder XRD was applied to determine the lattice evolution of $SbTaO_4$ up to 12.6 GPa (Figs. 3a–c). High-pressure powder XRD patterns can be well indexed to $SbTaO_4$, except for the peak around 9.1°. The impurity peak can be attributed to Ta_2O_5 (PDF #01–071–0639), which will not affect the optical property measurements. During compression, all Bragg diffraction peaks moved to the high-angle region, and no new Bragg diffraction peak emerged in the high-pressure XRD patterns, which indicated that the lattice of $SbTaO_4$ continues to shrink under this pressure region and no phase transition occurred. The evolution of cell parameters was also obtained by *Lebail* refinement, which demonstrated that the axial lengths *a*, *b*, and *c*, as well as the cell volume, continuously decrease under pressure. The cell volume was fitted to a second-order Birch-Murnaghan equation of state, in which $V_0 = 315.5(2)$ Å^3, $B_0 = 101.3(13)$ GPa. The bulk modulus B_0 of $SbTaO_4$ is lower than that of the α-phase Sb_2O_4 ($B_0 = 143$ GPa) and is compared to that of the β-phase Sb_2O_4 ($B_0 = 145$ GPa) [52], which own the similar crystal structures with $SbTaO_4$. High-pressure UV–vis absorption measurements were also executed to evaluate the absorption property and bandgap change up to 14.7 GPa (Fig. 3d and Fig. S8 in Supporting information). The absorption edge of $SbTaO_4$ exhibited a red shift during the compression process. Band gap shrinkage was also discovered, as band gap was reduced by ~15 % from 3.73 eV (ambient condition) to 3.17 eV (14.7 GPa), indicating a large pressure response on the electronic structure of $SbTaO_4$. High-pressure Raman measurement was also conducted up to 13.3 GPa (Fig. 3e). Raman peaks within the range of 100–500 cm^{-1} were prominently highlighted. These peaks can be identified as lattice vibrational modes. Additionally, pressure dependence of the Raman peak positions was displayed, and assignments were made for five strong peaks (Fig. 3f). It is noteworthy that softening phenomena occurs at the Raman peaks at 168.6 cm^{-1} (B_2) and 186.9 cm^{-1} (A_1), with rates of −1.3 cm^{-1}/GPa and −2.7 cm^{-1}/GPa, respectively. The vibrational modes of two softened peaks were visualized by first principles calculation (Fig. S9 in Supporting information), which demonstrated the lattice vibrations predominantly influenced by the LPE [SbO_4] unit. The softening phenomenon of Raman peaks suggests the distortion of the lattice in $SbTaO_4$ under pressure. The structural distortion of chromophores under pressure facilitates the formation of new STE states and modulates the relative intensities of different STE emissions, as reported in zero-dimensional metal halides [16,53].

Furtherly, combined with first-principles calculations, geometry optimization of $SbTaO_4$ under selected pressure was executed. Geometry optimization was adopted full relaxation method and equipped the initial structural model at ambient condition as the template for pressure calculation. Since the PL emission of $SbTaO_4$ originates from the $^1P_1$–$^1S_0$ transition mode in the LPE [SbO_4] unit, the evolution of the [SbO_4] unit after geometry optimization is focused. By extracting the Sb–O bond length and O–Sb–O bond angle of the [SbO_4] unit and quantifying the LPE [SbO_4] unit, two parameters of bond-angle deviation (δ^2) and bond-length deviation (λ) are calculated (Figs. 3g and h, Table S1 in Supporting information). Both increasing δ^2 and λ imply the enhanced distortion of the LPE [SbO_4] unit under pressure, which matches well with the pressure-driven softening phenomenon of Raman peaks. The enhanced distortion of the LPE [SbO_4] unit has remarkable impacts on excited-state distortion, which will hinder the transition pro-

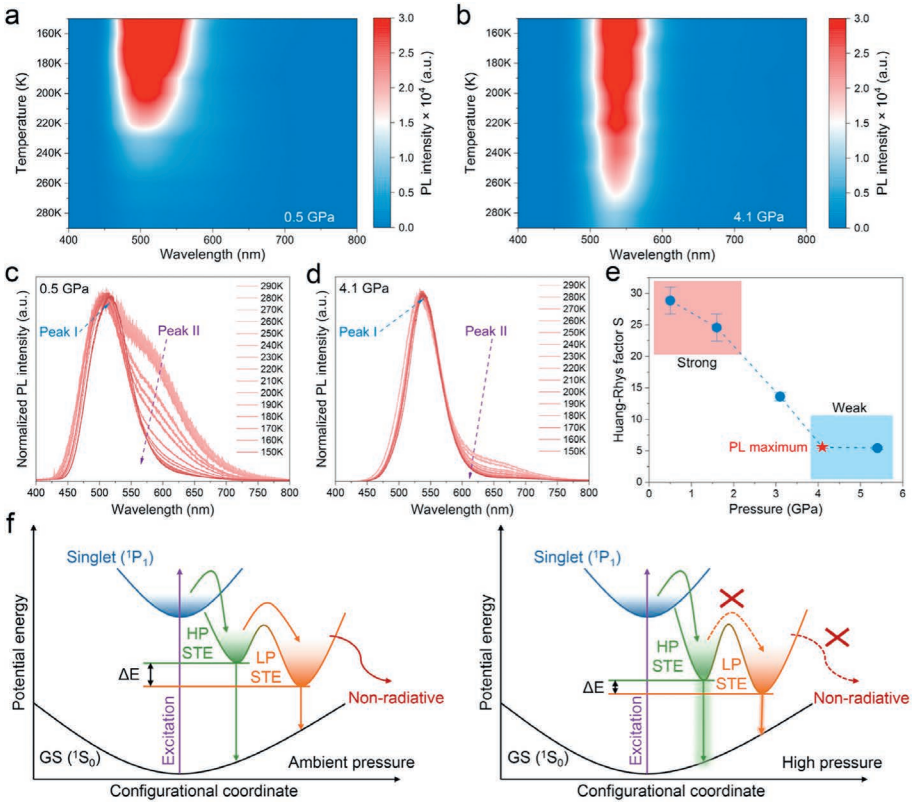


Fig. 4. (a, b) Temperature-dependent *pseudo*-color PL spectra under 0.5 and 4.1 GPa. (c, d) Normalized temperature-dependent PL spectra. (e) High-pressure evolution of the Huang-Rhys factor *S*. (f) Illustration of the STE emission mechanism upon compression.

cess from HP STE to LP STE, causing the enhancement of HP STE transition become faster than that of LP STE transition [16]. This is also the reason why the area ratio of peak I to peak II continuously increase.

Cryogenic PL spectra measurements under pressure were conducted at five pressure points: 0.5, 1.6, 3.1, 4.1, and 5.4 GPa, with the temperature ranging from 290 K to 150 K. Figs. 4a and b, Figs. S10a–c (Supporting information) point out that, as the temperature decreases, the intensity of the PL emission continuously enhances. The PL enhancement can be attributed to the characteristics of STE emission, where the low temperature suppresses non-radiative transitions, thereby promoting the PL emission. The cryogenic PL spectra at the five different pressure points are also normalized to further observe the evolutions of the PL emission (Figs. 4c and d, Figs. S10d–f in Supporting information). As the temperature decreases, the proportion of peak II in the overall PL emission gradually diminishes. This indicates that low temperature inhibits the transition from singlet HP STE to singlet LP STE, similar to the effect of pressure. Furthermore, Gaussian fitting is performed to analyze the FWHM of peak I, in order to understand the evolutions in electron-phonon coupling in $SbTaO_4$ under pressure. Electron-phonon coupling was obtained by the relationship between FWHM of peak I spectra according to the formula: $FWHM = 2.36\sqrt{S}\hbar\omega\sqrt{coth(\hbar\omega/2kT)}$, where ω is phonon frequency, $\hbar$ is reduced Planck constant, T is temperature, and k is Boltzmann constant. Based on this formula, Huang-Rhys factor S can be obtained (Fig. 4e and Fig. S11 in Supporting information), which reflects the strength of electron-phonon coupling of the material. At near atmospheric pressure (0.5 GPa), the Huang-Rhys factor S value of $SbTaO_4$ is 28.87. The large S implies strong electron-phonon coupling effect in $SbTaO_4$, which is the reason of broad PL emission, and the large S is comparable to those of halide perovskites and the recently reported ZnO nanocrystals [54,55]. Under pressure, the S value first decreases rapidly, and then remains stable at a lower value at 4.1 and 5.4 GPa. The weakening of Huang-Rhys factor S indicates the weakening of the electron-phonon coupling in $SbTaO_4$, which will lead to the suppression of non-radiative transitions in the transition process [55]. The inhibition of non-radiative transitions can also be demonstrated by the increased lifetimes of $SbTaO_4$ under pressure. Therefore, the inhibition of non-radiative transitions becomes another reason for the enhancement of PL emission in $SbTaO_4$.

Finally, two factors dominate the enhancement of the STE emission in $SbTaO_4$ under pressure: (1) The suppression of non-radiative transitions, and (2) the hindered transition from HP STE to LP STE. Fig. 4f clarifies the mechanism behind the bright PL emission of $SbTaO_4$ under pressure. At ambient pressure, due to the presence of self-trapped states within $SbTaO_4$, excitons drop from the free energy level ($^1P_1$) to self-trapped energy levels. At this time, because of the strong electron-phonon coupling in $SbTaO_4$, most of the energy is dissipated through non-radiative transitions and few of excitons return to the ground state ($^1S_0$) *via* HP STE and LP STE states, emitting weak green light. At high pressure, the electron-phonon coupling effect in $SbTaO_4$ weakens, leading to the suppression of non-radiative transitions. Consequently, more excitons opt to transition back to the ground state ($^1S_0$) *via* HP STE and LP STE states, which leads the enhancement of these PL emissions. Furthermore, the distortion of the LPE [SbO_4] units become stronger under pressure. This phenomenon reduces the energy difference (ΔE) between HP STE and LP STE states and then increases the barrier of excitons transitioning from HP STE to LP STE states, which hinders this transition process. These two factors cause the HP STE emission to be stronger than that of LP STE, resulting in bright green emission of $SbTaO_4$ under pressure. It was also observed that as the pressure continues to increase (5.8–13.2 GPa), the intensity of the PL emission weakens. This is

because pressure reduces the crystallinity of the sample, further suppressing the PL emission. This factor competes with the two PL-enhanced mechanisms mentioned above, and when the suppression of PL emission by pressure dominates, the PL emission weakens or even disappears [56].

In summary, $SbTaO_4$ exhibited a strong enhancement of the STE emission under pressure, and the bright green emission was achieved. The STE emission exhibited bi-peak characteristics, which can be split to HP STE (peak I) emission and LP STE (peak II) emission according to the energy difference. High-pressure time-resolved PL decay measurement revealed that the STE emission was caused by the $^1P_1-^1S_0$ transition in Sb^{3+} ions. The STE emission enhancement reached its maximum at 3.8 GPa, with peak I increasing ~20 times and peak II increasing ~3 times. The enhancement mechanism was explained by detailed high-pressure *in situ* measurements, including TA spectroscopy, Raman spectroscopy, cryogenic PL spectra and first-principles calculations. The STE emission enhancement can be attributed to the synergistic effects of two factors, *i.e.*, the suppression of non-radiative transitions and the hindered transition from HP STE to LP STE states. The weakening of the electron-phonon coupling suppresses non-radiative transitions, which enhances the whole PL emission. In addition, the distortion of the LPE [SbO_4] units hinders the transition from HP STE to LP STE states, which causes the enhancement of peak I is faster compared to peak II. The significant enhancement of STE emission in $SbTaO_4$ opens new avenues for high-pressure studies of STE emissions in inorganic oxides and highlights potential materials for advanced photonic devices operating under high-pressure conditions.

Declaration of competing interest

The authors declare that they have no known competing financial interests or personal relationships that could have appeared to influence the work reported in this paper.

CRediT authorship contribution statement

Dequan Jiang: Writing – original draft, Methodology, Data curation, Conceptualization. **Long Zhang:** Methodology, Conceptualization. **Chen Li:** Methodology. **Ke Liu:** Methodology. **Yingying Ma:** Methodology. **Hao-Ming Cheng:** Methodology. **Tianyao Pei:** Methodology. **En Chen:** Methodology. **Jianbo Zhang:** Methodology. **Ting Wen:** Methodology. **Yang Ding:** Supervision. **Yonggang Wang:** Writing – review & editing, Supervision, Funding acquisition.

Acknowledgments

This work was supported by the Major Program of the National Natural Science Foundation of China (No. 22090041), the National Natural Science Foundation of China (Nos. 52073003, 12204189), the Postdoctoral Fellowship Program of CPSF (No. GZC20230104) and the China Postdoctoral Science Foundation (No. 2023M730028). High-pressure XRD data were collected at the BL15U1 beamline of the Shanghai Synchrotron Radiation Facility (SSRF), Shanghai, China.

Supplementary materials

Supplementary material associated with this article can be found, in the online version, at doi:10.1016/j.cclet.2025.111264.

References

[1] M.D. Smith, H.I. Karunadasa, Acc. Chem. Res. 51 (2018) 619–627.
[2] X.K. Liu, W. Xu, S. Bai, et al., Nat. Mater. 20 (2021) 10–21.
[3] Q. Chen, J. Wu, X. Ou, et al., Nature 61 (2018) 88–93.
[4] Z. Li, H. Li, Y. Li, et al., Chin. Chem. Lett. 36 (2025) 109800.
[5] M.D. Smith, B.A. Connor, H.I. Karunadasa, Chem. Rev. 119 (2019) 3104–3139.
[6] Q. Guo, X. Zhao, B. Song, J. Luo, J. Tang, Adv. Mater. 34 (2022) 2201008.
[7] T. Hu, M.D. Smith, E.R. Dohner, et al., J. Phys. Chem. Lett. 7 (2016) 2258–2263.
[8] B.M. Benin, D.N. Dirin, V. Morad, et al., Angew. Chem. Int. Ed. 57 (2018) 11329–11333.
[9] S.R. Li, J.J. Luo, J. Liu, J. Tang, J. Phys. Chem. Lett. 10 (2019) 1999–2007.
[10] A. Noculak, V. Morad, K.M. McCall, et al., Chem. Mater. 32 (2020) 5118–5124.
[11] Y. Jing, Y. Liu, M. Li, Z. Xia, Adv. Optical Mater. 9 (2021) 2002213.
[12] Y. Deng, F. Li, Z. Zhou, et al., Chin. Chem. Lett. 35 (2024) 109085.
[13] K.M. McCall, V. Morad, B.M. Benin, M.V. Kovalenko, ACS Mater. Lett. 2 (2020) 1218–1232.
[14] C. Sun, Z. Deng, Z. Li, et al., Angew. Chem. Int. Ed. 62 (2023) e202216720.
[15] M. Li, Z. Xia, Chem. Soc. Rev. 50 (2021) 2626–2662.
[16] J. Han, Q. Li, B. Xu, et al., J. Mater. Chem. C 11 (2023) 10625–10633.
[17] V. Morad, S. Yakunin, M.V. Kovalenko, ACS Mater. Lett. 2 (2020) 845–852.
[18] C. Zhou, H. Lin, Y. Tian, et al., Chem. Sci. 9 (2018) 586–593.
[19] Z. Ma, Z. Shi, D. Yang, et al., ACS Energy Lett. 5 (2020) 385–394.
[20] Y. Jing, Y. Liu, X. Jiang, et al., Chem. Mater. 32 (2020) 5327–5334.
[21] J. Lin, P. Wang, J. Zhou, L. Mao, Angew. Chem. Int. Ed. 63 (2024) e202400554.
[22] B. Su, S. Geng, Z. Xiao, Z. Xia, Angew. Chem. Int. Ed. 61 (2022) e202208881.
[23] B. Su, M. Li, E. Song, Z. Xia, Adv. Funct. Mater. 31 (2021) 2105316.
[24] Q. Li, B. Xu, Z. Quan, Acc. Chem. Res. 56 (2023) 3282–3291.
[25] M.D. Smith, A. Jaffe, E.R. Dohner, A.M. Lindenberg, H.I. Karunadasa, Chem. Sci. 8 (2017) 4497–4504.
[26] G. Xiao, T. Geng, B. Zou, ACS Mater. Lett. 2 (2020) 1233–1239.
[27] H.K. Mao, X.J. Chen, Y. Ding, B. Li, L. Wang, Rev. Mod. Phys. 90 (2018) 015007.
[28] L. Zhang, K. Wang, Y. Lin, B. Zou, J. Phys. Chem. Lett. 11 (2020) 4693–4701.
[29] G. Niu, J. Jiang, X. Wang, et al., J. Phys. Chem. Lett. 15 (2024) 1623–1635.
[30] L. Zhang, C. Liu, L. Wang, et al., Angew. Chem. Int. Ed. 57 (2018) 11213–11217.
[31] Y. Wang, S. Guo, H. Luo, et al., J. Am. Chem. Soc. 142 (2020) 16001–16006.
[32] Q. Li, Z. Chen, B. Yang, et al., J. Am. Chem. Soc. 142 (2020) 1786–1791.
[33] S. Guo, Y. Zhao, K. Bu, et al., Angew. Chem. Int. Ed. 59 (2020) 17533–17539.
[34] Q. Li, Z. Chen, M. Li, et al., Angew. Chem. Int. Ed. 60 (2021) 2583–2587.
[35] L. Zhang, S. Li, H. Sun, et al., Angew. Chem. Int. Ed. 62 (2023) e202311912.
[36] Y. Liang, Y. Jiang, K.Z. Du, et al., Nano Lett. 23 (2023) 7599–7606.
[37] J. Liang, X. Mi, S. Guo, et al., Chin. J. Struct. Chem. 43 (2024) 100333.
[38] H.Y. Sang, J.F. Li, J. Alloy. Compd. 493 (2010) 678–682.
[39] Z. Yuan, P. Zheng, Y. Peng, et al., Phys. Rev. B 105 (2022) 014517.
[40] H. Mizoguchi, P. Chen, P. Boolchand, et al., Chem. Mater. 25 (2013) 3858–3866.
[41] V.I. Popolitov, L.A. Ivanova, S.Y. Stephanovitch, et al., Ferroelectrics 8 (1974) 519–520.
[42] W. Jeitschko, A.W. Sleight, Acta Cryst. B 30 (1974) 2088–2094.
[43] M. Wiegel, W. Middel, G. Blase, J. Mater. Chem. 5 (1995) 981–983.
[44] M. Zhang, L. Zhao, J. Xie, et al., Nat. Commun. 12 (2021) 4890.
[45] L. Niu, L. Zhao, D. Li, et al., Sci. China Chem. 66 (2023) 760–767.
[46] H.X. Qi, H. Jo, H.E. Lee, J. Hong, K.M. Ok, J. Solid State Chem. 274 (2019) 69–74.
[47] D.K. Das, R. Bakthavatsalam, V.R. Hathwar, R. Pallepogu, J. Kundu, J. Mater. Chem. C 11 (2023) 3855–3864.
[48] Q. Li, D. Zhou, J. Chai, et al., Nat. Commun. 11 (2020) 2897.
[49] P. Han, X. Zhang, C. Luo, et al., ACS Cent. Sci. 6 (2020) 566–572.
[50] P. Han, X. Mao, S. Yang, et al., Angew. Chem. Int. Ed. 58 (2019) 17231–17235.
[51] B. Yang, K. Han, J. Phys. Chem. Lett. 12 (2021) 8256–8262.
[52] D. Orosel, P. Balog, H. Liu, J. Qian, M. Jansen, J. Solid State Chem. 178 (2005) 2602–2607.
[53] Q. Li, B. Xu, Z. Chen, et al., Adv. Funct. Mater. 31 (2021) 2104923.
[54] R. Zhou, L. Sui, X. Liu, et al., Nat. Commun. 14 (2023) 1310.
[55] H. Luo, S. Guo, Y. Zhang, et al., Adv. Sci. 8 (2021) 2100786.
[56] L. Zhang, L. Wu, K. Wang, B. Zou, Adv. Sci. 6 (2019) 1801628.